JOURNAL OF CHEMICAL INFORMATION AND MODELING

Article

pubs.acs.org/jcim

Comparative Molecular Dynamics Studies of Human DNA Polymerase η

Melek N. Ucisik and Sharon Hammes-Schiffer*

Department of Chemistry, University of Illinois at Urbana−Champaign, 600 South Mathews Avenue, Urbana, Illinois 61801-3364, United States

Supporting Information

ABSTRACT: High-energy ultraviolet radiation damages DNA through the formation of cyclobutane pyrimidine dimers, which stall replication. When the lesion is a thymine−thymine dimer (TTD), human DNA polymerase η (Pol η) assists in resuming the replication process by inserting nucleotides opposite the damaged site. We performed extensive molecular dynamics (MD) simulations to investigate the structural and dynamical effects of four different Pol η complexes with or without a TTD and with either dATP or dGTP as the incoming base. No major differences in the overall structures and equilibrium dynamics were detected among the four systems, suggesting that the specificity of this enzyme is due predominantly to differences in local interactions in the binding regions. Analysis of the hydrogen-bonding interactions between the enzyme and the DNA and dNTP provided molecular-level insights. Specifically, the TTD was observed to engage in more hydrogen-bonding interactions with the enzyme than its undamaged counterpart of two normal thymines. The resulting greater rigidity and specific orientation of the TTD are consistent with the experimental observation of higher processivity and overall efficiency at TTD sites than at analogous sites with two normal thymines. The similarities between the systems containing dATP and dGTP are consistent with the experimental observation of relatively low fidelity with respect to the incoming base. Moreover, Q38 and R61, two strictly conserved amino acids across the Pol η family, were found to exhibit persistent hydrogen-bonding interactions with the TTD and cation-π interactions with the free base, respectively. Thus, these simulations provide molecular level insights into the basis for the selectivity and efficiency of this enzyme, as well as the roles of the two most strictly conserved residues.

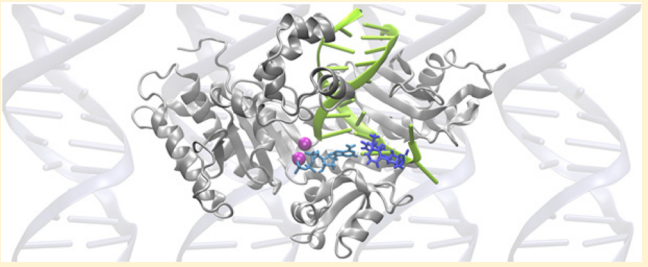

INTRODUCTION

The energy of the ultraviolet radiation from the sun is high enough to catalyze the formation of covalent bonds between adjacent pyrimidine bases in DNA, resulting in cyclobutane pyrimidine dimers (CPDs).[1,2] Such CPDs constitute one of the most prevalent types of DNA damage caused by exposure to sunlight.[3−6] This alteration of the pyrimidine nucleotides in DNA leads to structural and chemical changes in the vicinity of the CPD, modifying the Watson−Crick base pairing and base stacking. These changes are not tolerated by the high-fidelity, high-processivity DNA replication polymerases when these cells attempt to replicate, thereby resulting in stalled replication forks.[6−9] For the replication to continue and the genomic material to be correctly transferred to the new generation of cells, the CPD lesions need to be either excised and replaced with their undamaged counterparts or bypassed, a process by which the lesion itself is not repaired, but the primer strand retains accurate genomic information despite the damage in the template strand.[7,10−12] In the latter case, the Watson−Crick base pairing occurs correctly against the distorted nucleotides comprising the lesion, and the replication proceeds as usual. This process, denoted translesion DNA synthesis, is performed by specialized DNA polymerases, most of which are categorized as the Y-family DNA polymerases.[13−15] In humans, the Y-family encompasses four out of the 17 DNA polymerases: η, ι, κ, and Rev1. Each of these enzymes has different preferences in terms of the lesion and the incoming nucleotide that would be incorporated opposite the damaged bases.[16−18]

The bypass of cyclobutane thymine−thymine dimers (TTDs) is the specialty of DNA polymerase η, denoted Pol η, which is encoded by the human *POLH* gene.[19−22] Mutations in this gene cause the variant form of Xeroderma Pigmentosum, a condition characterized by deficiency of repairing sun-induced damage in skin, which in turn leads to increased sensitivity to sunlight and a high susceptibility to skin cancer.[23−27] Hence, the correct and complete functioning of Pol η is vital for humans. It binds to TTD-containing DNA more strongly than to undamaged DNA, and it exhibits higher accuracy and processivity when extending the DNA primer opposite a TTD than opposite two normal thymines.[28,29]

Despite its critical role in alleviating the negative effects of sun exposure, Pol η exhibits a few potentially disadvantageous properties that are common to the entire class of Y-family DNA

Received: October 2, 2015
Published: November 12, 2015

DOI: 10.1021/acs.jcim.5b00606
J. Chem. Inf. Model. 2015, 55, 2672−2681

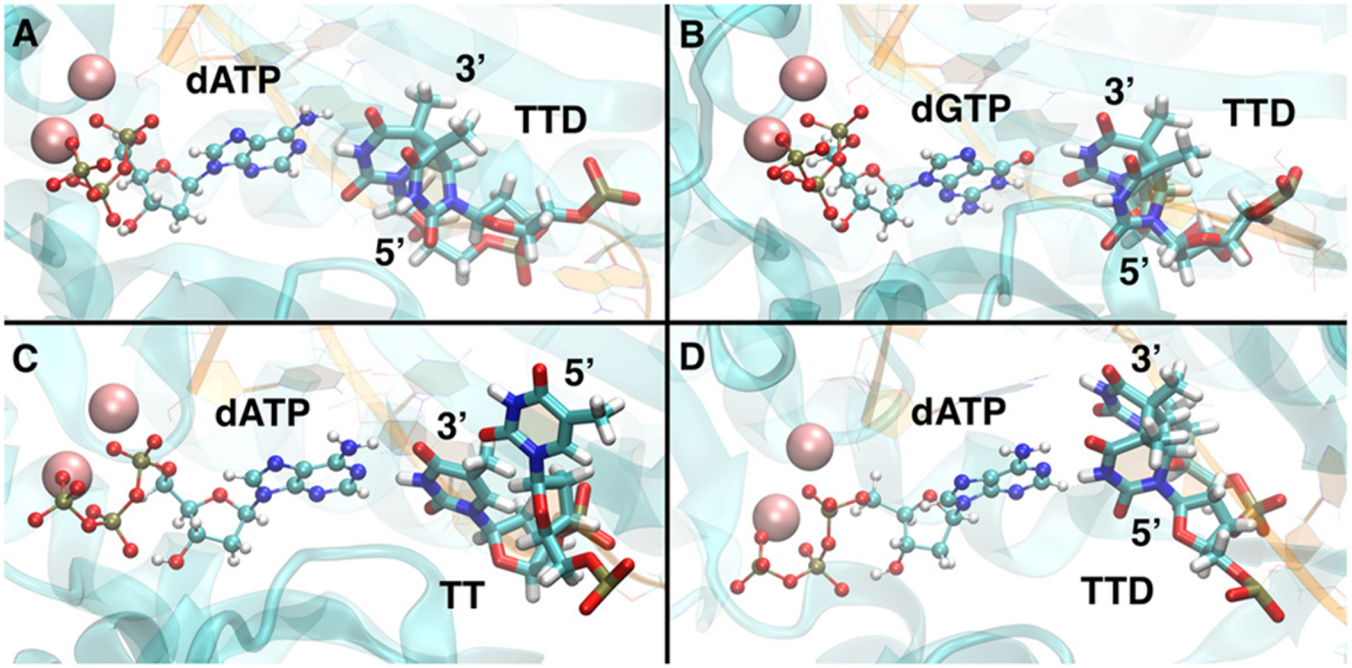

Figure 1. Active sites of the systems TTD3′-A (A), TTD3′-G (B), N/A-A (C), and TTD5′-A (D). The incoming free nucleotide, dATP or dGTP, is shown in ball-and-stick representation and labeled. The TTD or consecutive normal thymines for N/A-A is displayed in licorice representation with the 3′ and 5′ ends labeled.

polymerases. It incorporates incorrect bases frequently when operating on undamaged DNA, which could have severe mutational consequences.[30−32] Furthermore, it has a lower processivity and a lower catalytic efficiency than DNA replicases.[17] Thus, the use of Pol η for DNA replication is strictly regulated, and it is utilized only when the replication fork encounters a TTD.[21] In such cases, Pol η takes over the replication with its open active site to accommodate the bulky CPDs.[19,21] It also exhibits activity against the intrastrand cross-links in DNA that are induced by anticancer agents such as cisplatin, carboplatin, gemcitabine, and oxaliplatin. The activity of Pol η provides an opportunity for the cancer cells to proliferate further, rendering such chemotherapy less potent.[33−37] This resistance to cisplatin treatment could be decreased or even eradicated upon greater understanding of the structural and dynamical properties of Pol η.

In this paper, we present comparative molecular dynamics (MD) studies conducted on four systems comprised of the catalytic domain of Pol η, a DNA template/primer of six or eight base pairs with or without a TTD, and a free deoxyribose nucleotide triphosphate (dNTP), namely either dATP or dGTP.[19] The configurations generated along microsecond MD trajectories are extensively analyzed to elucidate the differences and similarities among the four systems. In particular, we investigate the hydrogen-bonding patterns in the region of the active site containing the incoming dNTP and the TTD or the two consecutive, normal thymines (TT) at the same location. These analyses provide insights into the structural and dynamical properties of Pol η that could be relevant to its critical function.

METHODS

We performed classical MD simulations on four systems comprised of the catalytic domain of the enzyme Pol η, a DNA primer/template of six or eight base pairs, and a free, incoming deoxyribose nucleotide triphosphate (dNTP). The enzyme consists of 432 amino acid residues and requires two Mg^{2+} ions for the nucleotidyl transfer reaction.[38] The four systems studied are as follows:

1. Pol η, an enzyme-bound DNA primer/template of eight base pairs with a TTD in its template strand, and a free deoxyribose adenine triphosphate (dATP) base-paired with the 3′ thymine of the TTD. This system is denoted "TTD3′-A" in our analysis, and the initial structure was obtained from the PDB structure 3MR3[19] with dAMNPP modified to dATP.
2. Pol η, an enzyme-bound DNA primer/template of eight base pairs with a TTD in its template strand, and a free deoxyribose guanine triphosphate (dGTP) base-paired with the 3′ thymine of the TTD. This system is termed "TTD3′-G" in our analysis, and the initial structure was obtained from the PDB structure 3MR3 with dAMNPP modified to dGTP to investigate the effects of a purine different from adenine, which is the natural Watson−Crick base-pair partner for thymine.
3. Pol η, an enzyme-bound DNA primer/template of six base pairs with no defect, and a free dATP base-paired with a normal thymine followed by another one located where the TTD would be. This system is denoted "N/A-A" in our analysis, and the initial structure was obtained from the PDB structure 3MR2[19] with dAMNPP modified to dATP.
4. Pol η, an enzyme-bound DNA primer/template of six base pairs with a TTD in its template strand, and a free dATP base-paired with the 5′ thymine of the TTD. This system is denoted "TTD5′-A" in our analysis, and the initial structure was obtained from the PDB structure 3SI8[19] with dAMNPP modified to dATP.

The complete DNA sequences and numbering are given in Table S1, and the entire complex for each system is depicted in

DOI: 10.1021/acs.jcim.5b00606
J. Chem. Inf. Model. 2015, 55, 2672−2681

Figure S1. The differences between these systems are highlighted in Figure 1.

These four systems were simulated with the ff12SB force field[39−42] for the protein and the ff99bsc0 force field for the DNA within the AMBER14 suite of programs.[43] All of the protein, nucleic acid, and solvent atoms were treated explicitly, and the Mg^{2+} parameters were adopted from Allner et al.[44] The Mg^{2+} ions were free to move but remained close to their original positions throughout the simulations. The atomic charges for the TTD and the dNTP residues, with N defined as A or G, were obtained using the restrained electrostatic potential (RESP) method.[45,46] The details pertaining to our RESP protocol and system preparation are provided in the SI. Each system was solvated with the TIP3P triangulated water model[47] in a periodically replicated truncated octahedral water box with sides that were at least 10 Å from any solute atom. The systems were neutralized by the addition of Na^+ ions, and then additional Na^+ and Cl^- ions were added to bring the salt concentration to ∼125 mM. The charged amino acids were modeled according to the protonation states obtained with the H++ protonation state server at neutral pH.[48]

Initially each system was processed through an energy-minimization protocol comprised of seven stages: the minimization of only the solvent atoms and the counterions (stage 1), the minimization of the solute hydrogen atoms (stage 2), the minimization of the side chains by gradually decreasing the harmonic positional restraints acting on them (stages 3−6), and finally the energy minimization of the whole system with no positional restraints (stage 7). A total of 63 000 energy-minimization steps were performed; the first 24 000 steps used the steepest descent method,[49] and the remaining 39 000 steps used the conjugate gradient method for minimization.[49] Subsequent to the energy minimization, a two-stage equilibration MD protocol was followed. First, the system was heated slowly from 0 to 300 K over 200 ps of MD within the canonical ensemble (NVT) while maintaining a weak harmonic restraint on the protein. Second, after the removal of the harmonic restraints, an MD trajectory of 10 ns at 300 K was propagated at a constant pressure of 1.0 bar within an isobaric, isothermal ensemble (NPT) using Langevin dynamics.[50]

Periodic boundary conditions were utilized for the energy minimizations and MD simulations. The Particle Mesh Ewald (PME) method was employed for long-range electrostatic interactions, and an 8 Å nonbonded cutoff was applied to limit the direct space sum in PME.[51] The lengths of the covalent bonds involving hydrogen were constrained with the SHAKE algorithm during the MD simulations.[52] The temperature of the systems was maintained at 300 K, and the pressure was maintained at 1.0 bar with Langevin dynamics with a collision frequency of 1.0 ps^{-1}. A time step of 2 fs was used for all MD trajectories.

Three independent, 1 μs MD trajectories were propagated within the NPT ensemble for each system beginning with the structures obtained from the second equilibration phase with random initial velocities chosen according to a Maxwell−Boltzmann distribution. The MD trajectories were analyzed to shed light on the structure and dynamics of the Pol η enzyme and the nucleic acids bound to it, namely the short DNA primer/template and the incoming dNTP. In this context, the term dynamics refers to equilibrium motions and fluctuations. Specifically, we performed a comprehensive analysis of key distances, root-mean-square deviations (RMSDs), root-mean-square fluctuations (RMSFs), radii of gyration, surface areas, nucleic acid flexibilities, and cross-correlations. These analyses were performed with the cpptraj utility of AmberTools13.[43]

RESULTS AND DISCUSSION

Structure and Motion of the Enzyme. To evaluate the structural stability over the MD trajectories, we examined the RMSDs of the C_α atoms of the protein backbone. Figure 2 overlays the RMSD profiles of the four systems using data from one MD trajectory per system. The RMSD analysis indicates that these systems are not fully equilibrated until ∼50 ns. Following this equilibration, the RMSD fluctuations within a trajectory remain within 1 Å, indicating that these are reasonably stable structures. The structural stability of the N/A-A system is comparable to that of the other three systems, suggesting that the presence of the TTD does not lead to extra stabilization that could have been related to the function of this enzyme.

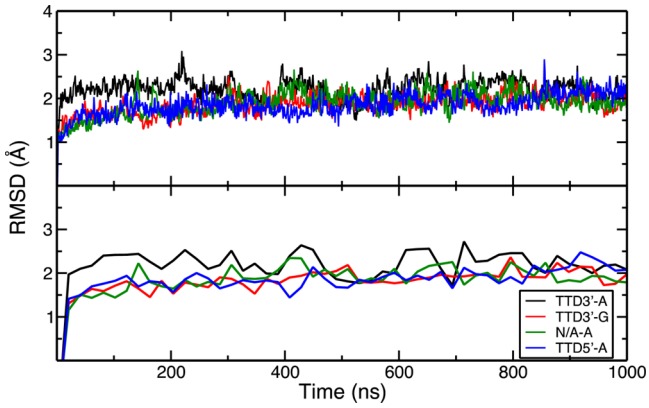

Figure 2. (top) RMSDs of the C_α atoms for the systems TTD3′-A (black), TTD3′-G (red), N/A-A (green), and TTD5′-A (blue) obtained from one of the three independent trajectories for each system. (bottom) Akima spline interpolations of the same data. The RMSDs obtained from all trajectories are provided in Figure S4.

The RMSDs of C_α atoms obtained from the three independent trajectories for each system are provided in Figure S4. The RMSD fluctuations within each trajectory remain within ∼1.5 Å for all 12 independent trajectories except for a jump observed in one of the TTD5′-A trajectories and another jump observed at the end of one of the TTD3′-G trajectories. The TTD5′-A trajectory jump can be traced to the thumb domain opening up in that trajectory. Specifically, one of the alpha helices contained within this domain becomes distorted, changing the packing of the helices and causing that whole domain to move slightly outward. The TTD3′-G trajectory jump can be attributed to the movement of the whole thumb domain toward the finger domain, a nearly opposite motion to what is observed for the TTD5′-A jump.

To locate the flexible regions of these four systems, we calculated the RMSFs of the C_α atoms. Figure 3 features an overlay of the RMSFs from one MD trajectory per system. The RMSFs for all three trajectories for each of the four systems are provided in Figure S5. The greatest mobility is found at the loop regions in the palm (residues 120−180) and little finger (residues 400−420) domains along with the entire thumb domain (residues 240−310), which consists of two longer alpha helices, one short α helix, and loops. The calculated RMSF plots are generally in agreement with the B-factors detected in the X-ray experiments for the TTD3′-A structure, as shown in

DOI: 10.1021/acs.jcim.5b00606
J. Chem. Inf. Model. 2015, 55, 2672−2681

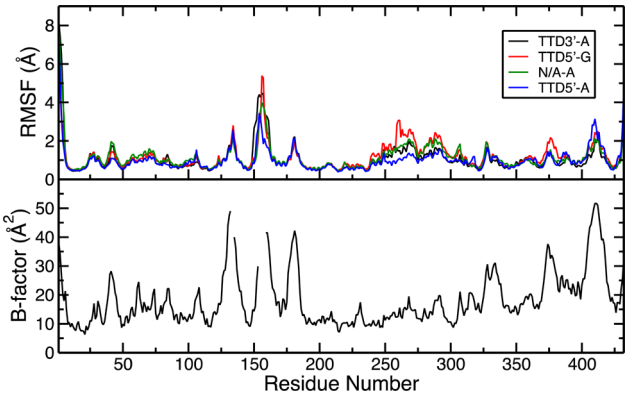

Figure 3. Comparison of the RMSFs of the four system from MD simulations and the B-factor values from the crystal structure 3MR3, which we used as the initial coordinates for the system TTD3′-A.

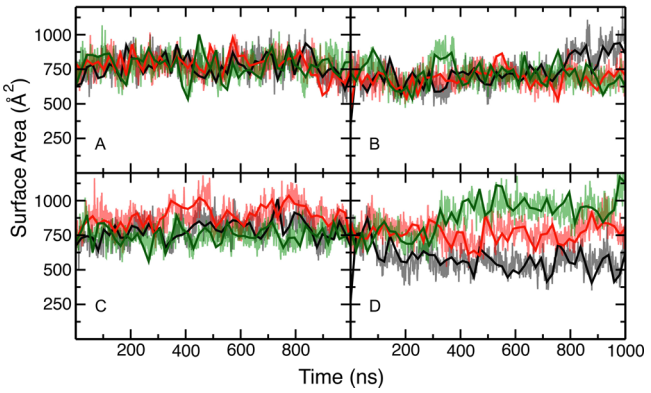

Figure 4. Surface areas for the consensus active site for all three independent trajectories of the four systems, TTD3′-A (A), TTD3′-G (B), N/A-A (C), and TTD5′-A (D), are shown as transparent lines, whereas the Akima spline interpolations of these are shown as thicker, opaque lines for better visibility of the trends. Black, red, and green represent the profiles for three independent trajectories.

Figure 3. However, the mobility of the thumb region is not as pronounced and the mobility of the little finger domain is more pronounced in the experiments than in the MD simulations.

The open active site of Pol η is believed to be one of the potential reasons for its low fidelity.[15,20,21] We investigated the time evolution of the binding surfaces of the DNA and the substrates, namely the dNTP molecules, during the MD trajectories. The molecular surface areas for the residues that directly participate in the nucleotidyl transfer reaction and the residues that interact closely with these residues were calculated using the linear combination of pairwise overlaps (LCPO) method by Weiser et al. as a function of time.[53] Initially this analysis was performed for the set of residues identified in ref 19. According to this previous work, the residues participating in the reaction are D13, M14, D115, and E116, which directly coordinate the two catalytic Mg^{2+} ions.[38] In addition, the residues F18, Q38, Y39, I48, R61, S62, K86, L89, Y92, and R93 were designated as residues interacting with the DNA and the dNTP around the active site. The surface area data for these residues are shown in Figures S6 and S7.

For a more comprehensive analysis, the definition of active site was modified to include all residues that are within 5 Å from the dNTP nucleotide or the TTD lesion (Table S2). These residues were inferred from three frames extracted from each of the TTD3′-A, TTD3′-G, and TTD5′-A MD trajectories. The identified residues for each system were combined to form a consensus active site, and the associated surface area was calculated for all 12 independent MD trajectories. The results are depicted in Figure 4. All of these trajectories initially exhibit a surface area value of approximately 750 Å^2. The TTD3′-A, TTD3′-G, and N/A-A trajectories oscillate about this value with minor fluctuations, with TTD3′-A remaining the most consistent. Two of the N/A-A trajectories exhibit a slightly more closed active site, which could be attributed to the absence of the distortion created by the TTD lesion. However, the difference is relatively small, thereby still consistent with a rather open active site spacious enough to accommodate distorted DNA.[15,21]

The greatest differences across the three trajectories for the same system are found in the TTD5′-A system, which corresponds to insertion of the second A opposite the 5′-T of the TTD by Pol η. For this system, the movement of the entire TTD deeper into the active site could possibly open up the binding pocket. The largest increase in the surface area is observed in the third trajectory of the TTD5′-A system, consistent with the significant change in the RMSD for this trajectory (Figure S4). Upon visual inspection, this increase in surface area appears to be due to the motion of the finger domain.

After investigating the active site surface area, we examined the overall compactness of the enzyme. For this purpose, we calculated the time evolution of the radius of gyration, as well as the largest distance between any two protein atoms, for the MD trajectories. As shown in Figure 5, all four systems exhibit

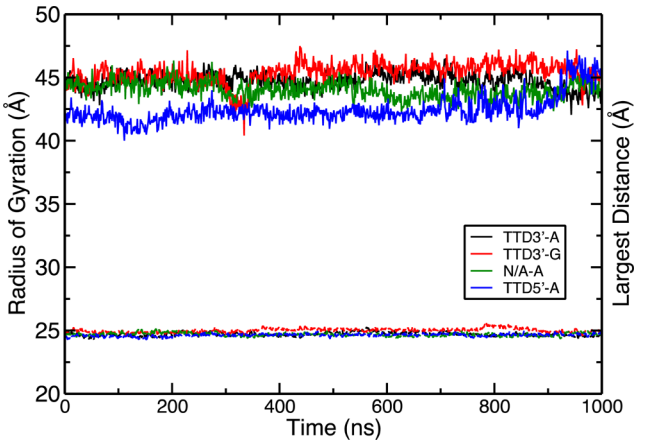

Figure 5. Time evolution of the radius of gyration (lower curves) and the largest distance between any two protein atoms (upper curves) for the systems TTD3′-A (black), TTD5′-G (red), N/A-A (green), and TTD5′-A (blue) obtained from one of the three independent trajectories for each system. The analogous data obtained from all trajectories are provided in Figure S5.

similar behavior with respect to these properties. The analogous data for all trajectories are provided in Figure S8. The compactness of these systems remains consistent throughout the trajectories with an approximate radius of gyration of 25 Å. The maximum interatomic distance is less meaningful than the radius of gyration because of the loop motions, but even this quantity remains mostly unchanged during the trajectories except for minor fluctuations.

To explore the possibility of correlated motions between distal residues in Pol η, we calculated the cross-correlation maps

DOI: 10.1021/acs.jcim.5b00606
J. Chem. Inf. Model. 2015, 55, 2672−2681

for all pairs of residues (Figure S9). In this analysis, correlated motions identify residues moving in the same direction, and anticorrelated motions identify residues moving in the opposite direction. No obvious pattern of correlations or anticorrelations was detected for these systems except for a few minor trends. Overall, these cross-correlation maps do not show any distinct interrelationship between motions across domains in this enzyme.

Structure and Motion of the Nucleic Acids. In this section, we analyze the structure and motion of the short DNA primer/template bound to Pol η and the free, incoming nucleotide, dNTP, where N is either A or G. Prior to this analysis, we ensured that the DNA strands across the four systems were superimposable. The set of base pairs C-G, G-C, T-A, C-G, and A-T are common to the primer/templates in all four systems, thereby allowing a comparison of their interactions with each other and with the environment. The DNA primer/template in 3SI8 has the same overall shape in the enzyme crevice, but the base pair sequence is structurally shifted upstream by one pair (Figure S10).

Geometric Configurations. To gain a better understanding of the geometric configurations of the DNA constructs bound to the enzyme in the four systems, we analyzed the nucleic acid flexibility parameters from the MD trajectories. The spatial arrangement of one base with respect to another within a base pair was examined through three rotational (buckle, propeller, opening) and three translational (shear, stretch, stagger) intrabase pair parameters. This examination showed that the base pairings were predominantly conserved, with the base pairs maintaining planarity, throughout the trajectories for each system.

Three translational (shift, slide, rise) and three rotational (tilt, roll, twist) interbase pair parameters were analyzed to obtain quantitative information about the spatial arrangement of the consecutive base pairs and thus the overall DNA structure. The slide and shift values were found to be small for all base pair steps in all systems, implying that the B-conformation of DNA was preserved at all times. The tilt and roll values were found to remain small during the simulated time frames, ensuring a mostly parallel arrangement of the base pairs throughout. Additionally, three translational (helical X-displacement, helical Y-displacement, helical rise) and three rotational (helical inclination, helical tip, helical twist) helix parameters were extracted from the MD trajectories. The X- and Y-displacement values were observed to be mostly around zero, and the rise values appeared as narrow distributions centered at ~3 Å. Inclination and tip angles were usually around 0°, and twist values displayed narrow distributions predominantly centered at around 35−40°. All of these findings support the overall observation of conservation of the B-form for the DNA strands bound to Pol η.

The major and minor groove widths of the DNA strands bound to Pol η were also examined. The time evolution of these widths is depicted in Figure 6 for one independent trajectory per system, and the data for all trajectories are provided in Figure S11. As depicted in Figure 6, these parameters remained extremely steady over the entire trajectory for systems N/A-A and TTD5′-A but exhibited wider fluctuations for systems TTD3′-A and TTD3′-G. These changes suggest that the DNA may be more mobile in the TTD3′-A and TTD3′-G systems.

Hydrogen Bonds. To characterize the significant interactions in these systems, we examined the number of hydrogen bonds formed within the nucleic acid subsystem, namely within the subsystem comprised of the DNA primer/template and the dNTP. To compare these numbers, Figures 7 and S12 depict histograms of the number of hydrogen bonds within the nucleic acid subsystem. Figure 7 illustrates that the nucleic acid construct in the TTD3′-A system forms the largest number of hydrogen bonds, suggesting stronger interactions between the DNA primer/template structure and the dNTP molecule. Interestingly, the smallest number of hydrogen bonds is found in the N/A-A system without a TTD.

The number of hydrogen bonds within the nucleic acid subsystem remains the lowest for the N/A-A system across the independent MD trajectories, as exhibited in the histograms given in Figure S12. Furthermore, all of the systems except for the TTD3′-G system form the same number of hydrogen bonds within the nucleic acid subsystem over the three independent trajectories, as demonstrated by the overlapping peaks in Figure S12. The greatest fluctuations are associated

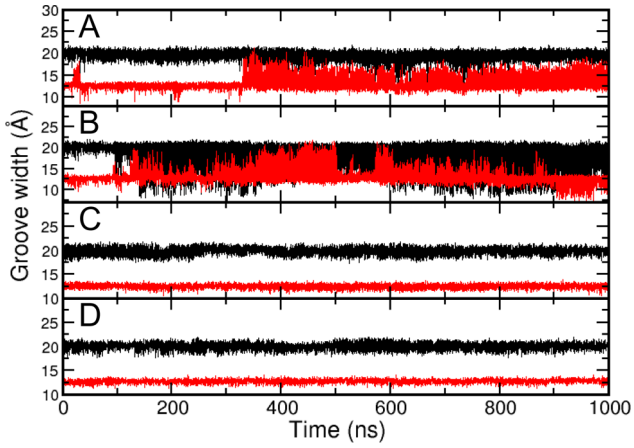

Figure 6. Time evolution of the major (black) and minor (red) groove widths for one of the three independent trajectories of the systems TTD3′-A (A), TTD3′-G (B), N/A-A (C), and TTD5′-A (D). The analogous data obtained from all trajectories are provided in Figure S11.

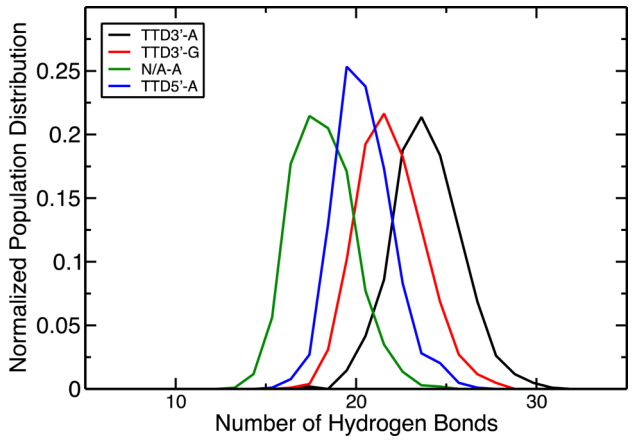

Figure 7. Histograms depicting the number of hydrogen bonds formed within the nucleic acids obtained from one of the three independent trajectories of the systems TTD3′-A (black), TTD3′-G (red), N/A-A (green), and TTD5′-A (blue). Hydrogen bonds were defined with a donor−acceptor heavy-atom distance cutoff of 3.5 Å and a donor−hydrogen−acceptor angle cutoff of 135°. The analogous data obtained from all trajectories are provided in Figure S12.

DOI: 10.1021/acs.jcim.5b00606
J. Chem. Inf. Model. 2015, 55, 2672−2681

with the only system containing dGTP rather than dATP. This observation could potentially be related to the substrate selectivity of Pol η.

In addition, the number of hydrogen bonds formed between the nucleic acids, i.e., the DNA primer/template or the dNTP, and the protein was quantified, as depicted in Figure 8. In

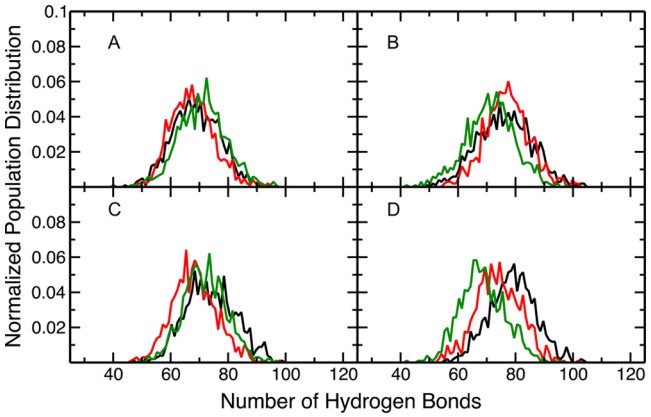

Figure 8. Histograms depicting the number of hydrogen bonds formed between the nucleic acids and the protein obtained from all three independent trajectories for the systems TTD3′-A (A), TTD3′-G (B), N/A-A (C), and TTD5′-A (D). The different colors represent independent trajectories.

contrast to the analysis above, the N/A-A system maintains almost the same number of hydrogen bonds between the DNA components and the amino acid residues as the other systems, indicating similar binding properties for the damaged and undamaged DNA to Pol η. Moreover, Figure 8 illustrates that approximately 50−100 hydrogen bonds are maintained between the nucleic acids and the protein during the entire time of the long MD trajectories. These persistent hydrogen-bonding interactions suggest that the DNA primer/template and dNTP are bound strongly to the protein in a relatively specific location and orientation. This observation could be related to the role of Pol η as a molecular splint, which was pointed out in previous experimental studies.[19] In particular, the enzyme is able to keep the damaged DNA template straight by accommodating TTD-induced distortions with only minor perturbations to the torsional angles of neighboring nucleotides, allowing the newly forming strand to preserve its B-form. If the template DNA around the lesion becomes distorted, it might not fit into the active site of Pol η and would either be left damaged, therefore stalling replication, or would need to be excised by the nucleotide-excision pair if it were recognized as damaged.

Hydrogen-Bonding Networks. We also investigated the details of the specific hydrogen-bonding network that holds the incoming free nucleotide and the TTD in place. Our analysis indicates that every lone pair with the potential of acting as a hydrogen bond acceptor on the dNTP is in close proximity to a possible hydrogen bond donor in the protein. This specific positioning of the dNTP with respect to the lesion may be related to the overall effectiveness of the nucleotidyl addition reaction in the case of TTD lesions.

For all four systems, the hydrogen bonds between dNTP and residues Y52, C16, F17, R55, and F18 are present in ∼70% or more of all saved configurations (Figure S13). The most common hydrogen bonds, which were detected in all trajectories, involve one of the oxygen atoms of the terminal phosphate in dNTP participating simultaneously in two hydrogen bonds. This oxygen atom establishes a hydrogen bond with the backbone amide of C16 in 99.8% of all saved configurations from all systems, with an average heavy-atom distance of 2.93 Å and an average angle of 164°. This same phosphate oxygen also exhibits a hydrogen bond with the side chain hydroxyl group of Y52 in 96.5% of all saved configurations with an average heavy-atom distance of 2.60 Å and an average angle of 167°. Previously mutations of Y52 were observed to alter the fidelity and efficiency of Pol η.[54,55] Similarly, the hydrogen atom attached to the backbone nitrogen of F17 and the guanidinium hydrogens of R55 form very persistent hydrogen bonds to triphosphate oxygens of the dNTP. Previously the R55A mutant of Pol η was found to be completely inactive.[54] The hydrogen bond involving the hydrogen attached to the backbone nitrogen of F18 and the deoxyribose O3′ is also observed in more than 75% of all saved configurations. In addition, hydrogen bonds were observed between the oxygens of the triphosphate of dNTP and the side chain amino hydrogens of K231, and occasionally between the N7 of dNTP and R61. The residues involved in these hydrogen-bonding interactions are depicted in Figure 9.

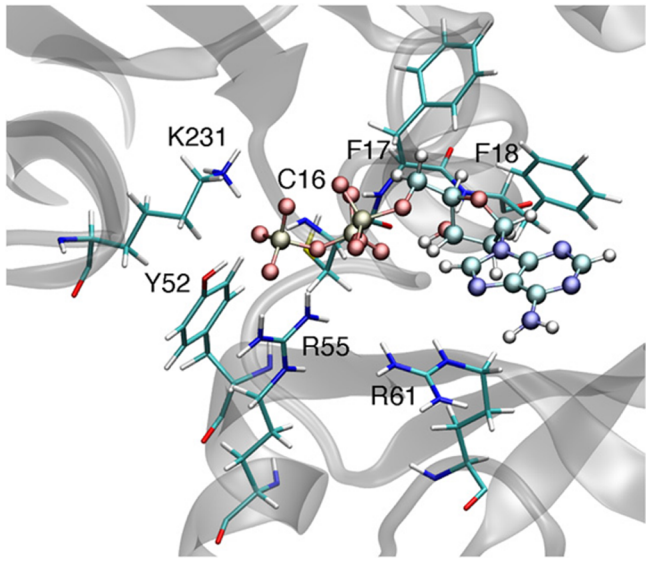

Figure 9. Depiction of the residues involved in the most common hydrogen-bonding interactions between the dNTP and Pol η: C16, F17, F18, Y52, R55, and R61, which are located in the finger domain, and K231, which is located in the palm domain. Mg^{2+} ions are not shown for clarity. The dNTP molecule is displayed in ball-and-stick representation, whereas the protein residues are represented as sticks.

In addition to these intermolecular hydrogen bonds holding the free dNTP in place, the two Mg^{2+} ions located near the triphosphate group may also contribute to the positioning of the dNTP. These combined effects create an electrostatic environment in which oppositely charged species are in close proximity and the triphosphate is fixed where it must be for the nucleotidyl addition reaction. The exact positioning and configuration of the dNTP are also maintained by a persistent intramolecular hydrogen bond between a phosphate oxygen and the O3′ hydrogen, as well as a persistent hydrogen bond between its O5′ and the O3′ hydrogen of the 3′ terminal nucleotide on the DNA primer. The structural stability of the

DOI: 10.1021/acs.jcim.5b00606
J. Chem. Inf. Model. 2015, 55, 2672−2681

dNTP is apparent from the RMSD and RMSF analyses (Figure S14 and Table S3). Although the average RMSFs of the dNTP range only from 0.23 to 0.31 Å across the four systems studied (Table S3), the RMSFs, as well as the fluctuations in the RMSD, are slightly lower in the TTD3′-A and TTD5′-A systems. These differences underscore the importance of the Watson−Crick base-pairing interactions that the dNTP base establishes with the TTD, where the interaction of A with T is expected to be stronger than the interaction of G with T.

Another hydrogen-bonding network is observed around the TTD. The occurrence of hydrogen bonds between the TTD and the protein is not as high as that of hydrogen bonds between the dNTP and the protein. The most recurrent hydrogen bond between the TTD and the protein involves residue Q38 through its side chain amide group. The hydrogen attached to the nitrogen of the side chain amide forms a hydrogen bond with the O2 atom of either thymine within the TTD. Residue Q38 establishes hydrogen bonds to the TTD in 34.4% of all saved snapshots with an average distance of 2.98 Å and an average angle of 156°. In some cases, it establishes two hydrogen bonds using both hydrogen atoms attached to the side chain amide nitrogen atom and the O2 atoms of both thymines of the TTD. This observation provides a possible explanation for the key role of residue Q38, as it is one of the two uniquely conserved amino acids in the entire Pol η family, and its substitution with Ala decreases the catalytic efficiency.[19] In addition to residue Q38, the protein residues A87, N324, Y39, R61, and R371 also form hydrogen-bonding interactions with the TTD or the TT motif in the N/A-A system in some configurations. The extent of hydrogen bonding around these thymines is much less in the absence of a TTD defect than in the presence of a TTD defect. In the absence of a TTD, the second thymine, which does not form a base pair with the incoming dNTP, can move freely due to the lack of steric constraints enforced by the covalent bonds constituting the cyclobutane moiety of the TTD. The enhanced mobility of the TT motif compared to the TTD motif is illustrated by our RMSD and RMSF analyses (Figure S15 and Table S3). Specifically, the average RMSF of the TT in the N/A-A system is 0.97 Å, whereas the average RMSF of the TTD in the other three systems ranges from 0.38 to 0.59 Å. This decrease in hydrogen-bonding interactions between the normal TT motif and the protein could contribute to the reduced overall efficiency in nucleotidyl addition reactions for undamaged DNA.

In addition to residue Q38, residue R61 is the second strictly conserved amino acid in the Pol η family of enzymes.[19] It exhibits a persistent cation-π interaction with the incoming dNTP molecule as well as less persistent hydrogen-bonding interactions between its guanidium hydrogens and the nitrogen or oxygen atoms of the dNTP. Such cation-π interactions involving arginine residues are fairly common in proteins.[56,57] In 83.2−95.8% of all saved configurations for the four systems, the distance between the central carbon of the guanidinium side chain and the center of mass of the purine heavy atoms was found to be less than 6 Å, which strongly suggests a cation-π interaction when combined with our thorough visual analysis. In contrast to the claim in ref 19, the closed finger domain was not observed to block residue R61 from stacking with the purine base.[19] This situation is related to the observation that residue R61 forms cation-π interactions with the base of the dNTP molecule in the crystal structures of the yeast Pol η-cisPt-DNA complex.[58]

Another factor to explore is the extent of hydrogen bonding between the incoming nucleotide dNTP and the TTD. For the TTD3′-A, TTD3′-G, and TTD5′-A systems, Watson−Crick base pairing between one of the T residues of the TTD and the purine base of the dNTP is observed. These hydrogen bonds are mostly conserved throughout the trajectories for these systems. For the N/A-A system, the Watson−Crick base pairing involves the dATP and the 3′ thymine residue opposite it, although the hydrogen bonds associated with this base pairing disappear occasionally during the trajectories. In this case, either the dATP forms weak interactions with the 5′ thymine or does not pair with any bases.

Additional Observations. As a further analysis, we examined the physical positioning of dNTP and the 3′ terminus of the DNA primer to determine if any of the systems at hand would favor the nucleophilic attack by the O3′ atom of the 3′-end of the DNA primer on the α-phosphate (P_α) of the dNTP molecule. The separation between these two atoms remains between 2.9 and 3.6 Å throughout all of the trajectories. The most prevalent value for this distance is 3.1−3.2 Å, as illustrated in Figure S16. Hence, none of the four systems exhibits an advantage or a disadvantage in terms of the ease of the nucleophilic attack. The relative positions of the dNTP and the 3′-DNA primer remain virtually the same in all four systems.

Finally, we performed an analysis of the atomic fluctuations of the phosphorus atoms of the DNA backbone to investigate the relative mobilities of the nucleotides in the DNA strands. Note that the 5′-terminal nucleotides are exempt from this analysis because of their lack of phosphate groups. In the template strand, the mobility is consistently low in the region around the TTD, as depicted in Figures 10 and S17. In general, the nucleotides toward the strand ends are more mobile. Overall, the residues that are closer to the active site are less mobile, as they are embedded in a more extended hydrogen-bonding network involving not only their phosphate groups, but also the thymine bases themselves. Additionally, covalent bonding enforces restraints on the motions of the thymines of

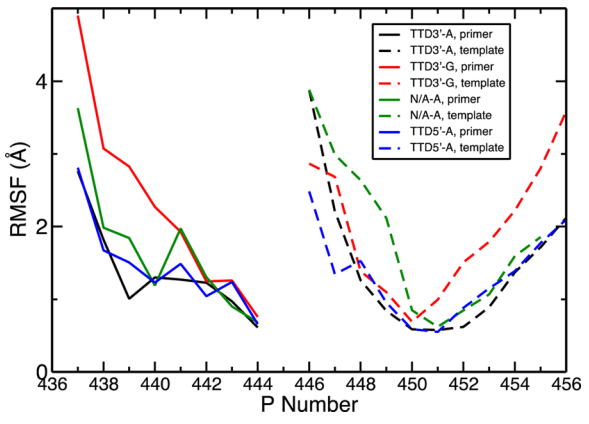

Figure 10. RMSFs of the P atoms in the DNA constructs in systems TTD3′-A (black), TTD3′-G (red), N/A-A (green), and TTD5′-A (blue) from one of the three independent trajectories. The primer strands are represented as solid lines and the template strands are represented as dashed lines. P atoms 447 and 448 represent the P atoms of the TTD in the TTD3′-A and TTD3′-G systems, while P atoms 448 and 449 constitute the TTD in the TTD5′-A and the normal TT in the N/A-A systems. The analogous data for all trajectories are depicted in Figure S17.

DOI: 10.1021/acs.jcim.5b00606
J. Chem. Inf. Model. 2015, 55, 2672−2681

the TTD, as illustrated by the typically lower mobilities of the P1 and P2 atoms of the TTD3′-A, TTD3′-G, and TTD5′-A systems compared to the P atoms of residues 448 and 449 in the N/A-A system (Figure S17).

CONCLUSIONS

In this paper, we used classical MD to explore the structure and dynamics of four different systems containing the catalytic domain of the enzyme Pol η, a DNA primer/template bound to the enzyme, and a free dNTP molecule in its active site. The bound DNA has a TTD in only three of the four systems to assess the effects of damaged versus undamaged DNA, while the dNTP is either dATP or dGTP to determine the impact of the purine base identity. We specifically sought a molecular level explanation for the low fidelity and processivity of Pol η in the absence of a TTD in the bound template DNA strand. Previously, in vitro studies observed both of these properties to increase significantly if the enzyme was acting upon DNA templates with cyclobutane pyrimidine dimers, especially TTDs.[28−31] An objective of this work was to determine if this improvement could arise from structural and dynamical differences in Pol η depending on the presence or absence of a TTD.

We generated a total of 3 μs of classical MD data on each of the four Pol η-DNA-dNTP systems through three independent 1 μs trajectories. Analyses of the RMSD, RMSF, active site surface area, radius of gyration, and cross-correlation maps for the enzyme, in conjunction with analyses of nucleic acid flexibility, major/minor groove width, nucleophilic attack distance for the nucleotidyl addition reaction, RMSF, cation-π interaction, and hydrogen-bonding networks for the bound DNA and dNTP, identified only minor differences in the overall structures and equilibrium dynamics among the four systems studied. A notable exception to this similarity among the four systems is the hydrogen-bonding patterns around the TTD and between the dNTP and the TTD or, for one system, the two consecutive, normal thymines at the same location as the TTD. The Y52, C16, F17, R55, and F18 residues were found to form the most persistent hydrogen bonds with the dNTP, regardless of the purine base identity. On the other hand, the TTD was found to participate in a higher number of hydrogen bonds with the enzyme than its healthy counterpart of two normal thymines, thereby potentially leading to a stronger binding interaction between the enzyme and the TTD. The Q38 residue established the most persistent hydrogen bond with the TTD, underscoring its importance as one of the two strictly conserved residues in the Pol η family. Moreover, the second strictly conserved R61 residue was observed to form persistent cation-π interactions with the purine base of the dNTP, also providing an indication of its key role.

Our findings are consistent with the low fidelity of Pol η with respect to the base of the incoming dNTP molecule[28−31] because no significant differences were detected between the structures and dynamics of the systems containing dATP versus dGTP. The structural and dynamical similarities suggest that the enzyme may not be able to easily differentiate between dATP and dGTP, therefore potentially leading to replication errors. Furthermore, the observed differences in hydrogen-bonding interactions between the DNA primer/template and the enzyme in the absence or presence of the TTD could explain the elevated overall efficiency of the enzyme in the presence of a TTD defect.[19,29] In particular, the covalently bonded thymines comprising a cyclobutane dimer were found to be held more tightly in place than their normal counterparts through a more extensive hydrogen-bonding network. Pol η appears to be designed to hold the TTD defect region more rigidly than most nucleotides bound to its DNA-binding interface, although its base pair partner, the dNTP molecule, is not covalently bonded to the upstream DNA primer yet. This more rigid and specific orientation could contribute to the elevated bypass efficiency of the enzyme in the presence of a TTD lesion.

The results from these MD trajectories provided the groundwork for another study focusing on the relative binding free energies of dATP and dGTP to the enzyme-TTD or enzyme-TT complex.[59] The relative binding free energies for these systems were explained through differences in hydrogen-bonding interactions observed during the microsecond MD trajectories. The conclusion from the present study that the overall structure and dynamics of the protein are similar for the TTD versus the normal TT and the dATP versus dGTP systems provides support for explaining the differences in binding free energies in terms of local interactions in the binding regions. In particular, the more persistent hydrogen-bonding interactions between the enzyme and the TTD provide a molecular-level explanation for the greater binding free energy of dATP to the TTD-containing DNA than to the undamaged DNA. Analysis of the hydrogen-bonding interactions between the DNA and the incoming base provided additional insights into the greater binding free energy of dATP versus dGTP to the enzyme−DNA complex. These types of comparative studies are enhancing our understanding of the molecular basis for the fidelity and overall efficiency of this biomedically important enzyme. A molecular-level understanding of this system could assist in the design of inhibitors to improve the effectiveness of cancer chemotherapy treatments for skin cancer in the future.[33,34,36,58]

ASSOCIATED CONTENT

Supporting Information

The Supporting Information is available free of charge on the ACS Publications website at DOI: 10.1021/acs.jcim.5b00606.

3D models of the systems; sequence, secondary structure, and domain information on Pol η; protocol for obtaining the charges for the TTD, dATP, dGTP residues with RESP; detailed structure preparation protocol for MD simulations; plots showing the RMSD, RMSF, surface area, radius of gyration, cross-correlation maps and hydrogen-bond analysis in all trajectories; tables of the sequences of bound DNA to Pol η; tables with the descriptions of consensus active sites used in analyses; tables with substrate and TTD RMSF information (PDF)

AUTHOR INFORMATION

Corresponding Author

*Telephone: (217) 300-0335. E-mail: shs3@illinois.edu (S.H.-S.).

Notes

The authors declare no competing financial interest.

ACKNOWLEDGMENTS

This work was funded by National Institutes of Health grant GM056207. The authors thank Dr. Alexander Soudackov, Dr. Wei Yang, Dr. Philip Hanoian, Dr. Steven Benkovic, and Dr.

DOI: 10.1021/acs.jcim.5b00606
J. Chem. Inf. Model. 2015, 55, 2672−2681

Jason Swails for helpful discussions. They also acknowledge computing support from Extreme Science and Engineering Discovery Environment (XSEDE).

REFERENCES

(1) Durbeej, B.; Eriksson, L. A. Reaction Mechanism of Thymine Dimer Formation in DNA Induced by Uv Light. *J. Photochem. Photobiol., A* **2002**, *152*, 95−101.
(2) Goodsell, D. S. The Molecular Perspective: Ultraviolet Light and Pyrimidine Dimers. *Oncologist* **2001**, *6*, 298−299.
(3) Mouret, S.; Baudouin, C.; Charveron, M.; Favier, A.; Cadet, J.; Douki, T. Cyclobutane Pyrimidine Dimers Are Predominant DNA Lesions in Whole Human Skin Exposed to Uva Radiation. *Proc. Natl. Acad. Sci. U. S. A.* **2006**, *103*, 13765−13770.
(4) Rochette, P. J.; Therrien, J. P.; Drouin, R.; Perdiz, D.; Bastien, N.; Drobetsky, E. A.; Sage, E. Uva-Induced Cyclobutane Pyrimidine Dimers Form Predominantly at Thymine-Thymine Dipyrimidines and Correlate with the Mutation Spectrum in Rodent Cells. *Nucleic Acids Res.* **2003**, *31*, 2786−2794.
(5) Mullenders, L. H. F.; Dokkum, A. M. H.; Kalle, W. H. J.; Vrieling, H.; Zdzienicka, M. Z.; Vanzeeland, A. A. Uv-Induced Photolesions, Their Repair and Mutations. *Mutat. Res., Genet. Toxicol. Test.* **1993**, *299*, 271−276.
(6) You, Y. H.; Lee, D. H.; Yoon, J. H.; Nakajima, S.; Yasui, A.; Pfeifer, G. P. Cyclobutane Pyrimidine Dimers Are Responsible for the Vast Majority of Mutations Induced by Uvb Irradiation in Mammalian Cells. *J. Biol. Chem.* **2001**, *276*, 44688−44694.
(7) Wood, R. D.; Araujo, S. J.; Ariza, R. R.; Batty, D. P.; Biggerstaff, M.; Evans, E.; Gaillard, P. H.; Gunz, D.; Koberle, B.; Kuraoka, I.; Moggs, J. G.; Sandall, J. K.; Shivji, M. K. K. DNA Damage Recognition and Nucleotide Excision Repair in Mammalian Cells. *Cold Spring Harbor Symp. Quant. Biol.* **2000**, *65*, 173−182.
(8) Yang, W. Structure and Mechanism for DNA Lesion Recognition. *Cell Res.* **2008**, *18*, 184−197.
(9) Yang, W. Poor Base Stacking at DNA Lesions May Initiate Recognition by Many Repair Proteins. *DNA Repair* **2006**, *5*, 654−666.
(10) Sale, J. E. Competition, Collaboration and Coordination - Determining How Cells Bypass DNA Damage. *J. Cell Sci.* **2012**, *125*, 1633−1643.
(11) Boiteux, S.; Jinks-Robertson, S. DNA Repair Mechanisms and the Bypass of DNA Damage in Saccharomyces Cerevisiae. *Genetics* **2013**, *193*, 1025−1064.
(12) Budzowska, M.; Kanaar, R. Mechanisms of Dealing with DNA Damage-Induced Replication Problems. *Cell Biochem. Biophys.* **2009**, *53*, 17−31.
(13) Livneh, Z.; Ziv, O.; Shachar, S. Multiple Two-Polymerase Mechanisms in Mammalian Translesion DNA Synthesis. *Cell Cycle* **2010**, *9*, 729−735.
(14) Wang, F.; Yang, W. Structural Insight into Translesion Synthesis by DNA Pol II. *Cell* **2009**, *139*, 1279−1289.
(15) Yang, W.; Woodgate, R. What a Difference a Decade Makes: Insights into Translesion DNA Synthesis. *Proc. Natl. Acad. Sci. U. S. A.* **2007**, *104*, 15591−15598.
(16) Ohmori, H.; Friedberg, E. C.; Fuchs, R. P. P.; Goodman, M. F.; Hanaoka, F.; Hinkle, D.; Kunkel, T. A.; Lawrence, C. W.; Livneh, Z.; Nohmi, T.; Prakash, L.; Prakash, S.; Todo, T.; Walker, G. C.; Wang, Z. G.; Woodgate, R. The Y-Family of DNA Polymerases. *Mol. Cell* **2001**, *8*, 7−8.
(17) Sale, J. E.; Lehmann, A. R.; Woodgate, R. Y-Family DNA Polymerases and Their Role in Tolerance of Cellular DNA Damage. *Nat. Rev. Mol. Cell Biol.* **2012**, *13*, 141−152.
(18) Maxwell, B. A.; Suo, Z. C. Recent Insight into the Kinetic Mechanisms and Conformational Dynamics of Y-Family DNA Polymerases. *Biochemistry* **2014**, *53*, 2804−2814.
(19) Biertumpfel, C.; Zhao, Y.; Kondo, Y.; Ramon-Maiques, S.; Gregory, M.; Lee, J. Y.; Masutani, C.; Lehmann, A. R.; Hanaoka, F.; Yang, W. Structure and Mechanism of Human DNA Polymerase *η*. *Nature* **2010**, *465*, 1044−1048.
(20) Cruet-Hennequart, S.; Gallagher, K.; Sokòl, A.; Villalan, S.; Prendergast, Á.; Carty, M. DNA Polymerase *η*, a Key Protein in Translesion Synthesis in Human Cells. In *Subcell Biochemistry*; Nasheuer, H.-P., Ed.; Springer: Netherlands, 2010; Vol. *50*, Chapter 10, pp 189−209.
(21) Yang, W. An Overview of Y-Family DNA Polymerases and a Case Study of Human DNA Polymerase *η*. *Biochemistry* **2014**, *53*, 2793−2803.
(22) Masutani, C.; Kusumoto, R.; Iwai, S.; Hanaoka, F. Mechanisms of Accurate Translesion Synthesis by Human DNA Polymerase *η*. *EMBO J.* **2000**, *19*, 3100−3109.
(23) Cleaver, J. E. Xeroderma Pigmentosum - Variants with Normal DNA-Repair and Normal Sensitivity to Ultraviolet-Light. *J. Invest. Dermatol.* **1972**, *58*, 124−128.
(24) Johnson, R. E.; Kondratick, C. M.; Prakash, S.; Prakash, L. HRAD30 Mutations in the Variant Form of Xeroderma Pigmentosum. *Science* **1999**, *285*, 263−265.
(25) Hanaoka, F.; Kusumoto, R.; Yamada, A.; Dohmae, N.; Yokoi, M.; Yuasa, M.; Araki, M.; Iwai, S.; Takio, K.; Masutani, C. The XPV (Xeroderma Pigmentosum Variant) Gene Encodes Human DNA Polymerase *η*. *Nature* **1999**, *399*, 700−704.
(26) Brash, D. E. Sunlight and the Onset of Skin Cancer. *Trends Genet.* **1997**, *13*, 410−414.
(27) de Gruijl, F. R. Skin Cancer and Solar UV Radiation. *Eur. J. Cancer* **1999**, *35*, 2003−2009.
(28) Kusumoto, R.; Masutani, C.; Shimmyo, S.; Iwai, S.; Hanaoka, F. DNA Binding Properties of Human DNA Polymerase *η*: Implications for Fidelity and Polymerase Switching of Translesion Synthesis. *Genes Cells* **2004**, *9*, 1139−1150.
(29) McCulloch, S. D.; Kokoska, R. J.; Masutani, C.; Iwai, S.; Hanaoka, F.; Kunkel, T. A. Preferential Cis-Syn Thymine Dimer Bypass by DNA Polymerase *η* Occurs with Biased Fidelity. *Nature* **2004**, *428*, 97−100.
(30) Johnson, R. E.; Washington, M. T.; Prakash, S.; Prakash, L. Fidelity of Human DNA Polymerase *η*. *J. Biol. Chem.* **2000**, *275*, 7447−7450.
(31) Kunkel, T. A.; Bebenek, K.; Masutani, C.; Hanaoka, F.; Matsuda, T. Low Fidelity DNA Synthesis by Human DNA Polymerase *η*. *Nature* **2000**, *404*, 1011−1013.
(32) Boudsocq, F.; Ling, H.; Yang, W.; Woodgate, R. Structure-Based Interpretation of Missense Mutations in Y-Family DNA Polymerases and Their Implications for Polymerase Function and Lesion Bypass. *DNA Repair* **2002**, *1*, 343−358.
(33) Cruet-Hennequart, S.; Villalan, S.; Kaczmarczyk, A.; O'Meara, E.; Sokol, A. M.; Carty, M. P. Characterization of the Effects of Cisplatin and Carboplatin on Cell Cycle Progression and DNA Damage Response Activation in DNA Polymerase *η*-Deficient Human Cells. *Cell Cycle* **2009**, *8*, 3043−3054.
(34) Ummat, A.; Rechkoblit, O.; Jain, R.; Choudhury, J. R.; Johnson, R. E.; Silverstein, T. D.; Buku, A.; Lone, S.; Prakash, L.; Prakash, S.; Aggarwal, A. K. Structural Basis for Cisplatin DNA Damage Tolerance by Human Polymerase *η* During Cancer Chemotherapy. *Nat. Struct. Mol. Biol.* **2012**, *19*, 628−632.
(35) Vaisman, A.; Masutani, C.; Hanaoka, F.; Chaney, S. G. Efficient Translesion Replication Past Oxaliplatin and Cisplatin GpG Adducts by Human DNA Polymerase *η*. *Biochemistry* **2000**, *39*, 4575−4580.
(36) Zhao, Y.; Biertumpfel, C.; Gregory, M. T.; Hua, Y. J.; Hanaoka, F.; Yang, W. Structural Basis of Human DNA Polymerase *η*-Mediated Chemoresistance to Cisplatin. *Proc. Natl. Acad. Sci. U. S. A.* **2012**, *109*, 7269−7274.
(37) Parsons, J. L.; Nicolay, N. H.; Sharma, R. A. Biological and Therapeutic Relevance of Nonreplicative DNA Polymerases to Cancer. *Antioxid. Redox Signaling* **2013**, *18*, 851−873.
(38) Nakamura, T.; Zhao, Y.; Yamagata, Y.; Hua, Y. J.; Yang, W. Watching DNA Polymerase *η* Make a Phosphodiester Bond. *Nature* **2012**, *487*, 196−U77.
(39) Cornell, W. D.; Cieplak, P.; Bayly, C. I.; Gould, I. R.; Merz, K. M.; Ferguson, D. M.; Spellmeyer, D. C.; Fox, T.; Caldwell, J. W.; Kollman, P. A. A Second Generation Force Field for the Simulation of

DOI: 10.1021/acs.jcim.5b00606
J. Chem. Inf. Model. 2015, 55, 2672−2681

Proteins, Nucleic Acids, and Organic Molecules. *J. Am. Chem. Soc.* **1995**, *117*, 5179−5197.
(40) Cheatham, T. E.; Cieplak, P.; Kollman, P. A. A Modified Version of the Cornell et al. Force Field with Improved Sugar Pucker Phases and Helical Repeat. *J. Biomol. Struct. Dyn.* **1999**, *16*, 845−862.
(41) Perez, A.; Marchan, I.; Svozil, D.; Sponer, J.; Cheatham, T. E.; Laughton, C. A.; Orozco, M. Refinenement of the Amber Force Field for Nucleic Acids: Improving the Description of Alpha/Gamma Conformers. *Biophys. J.* **2007**, *92*, 3817−3829.
(42) Hornak, V.; Abel, R.; Okur, A.; Strockbine, B.; Roitberg, A.; Simmerling, C. Comparison of Multiple Amber Force Fields and Development of Improved Protein Backbone Parameters. *Proteins: Struct., Funct., Genet.* **2006**, *65*, 712−725.
(43) Case, D. A.; Babin, V.; Berryman, J. T.; Betz, R. M.; Cai, Q.; Cerutti, D. S.; Cheatham III, T. E.; Darden, T. A.; Duke, R. E.; Gohlke, H.; Goetz, A. W.; Gusarov, S.; Homeyer, N.; Janowski, P.; Kaus, J.; Kolossváry, I.; Kovalenko, A.; Lee, T. S.; LeGrand, S.; Luchko, T.; Luo, R.; Madej, B.; Merz, K. M.; Paesani, F.; Roe, D. R.; Roitberg, A.; Sagui, C.; Salomon-Ferrer, R.; Seabra, G.; Simmerling, C. L.; Smith, W.; Swails, J.; Walker, R. C.; Wang, J.; Wolf, R. M.; Wu, X.; Kollman, P. A. *Amber 14*; University of California, San Francisco, 2014.
(44) Allner, O.; Nilsson, L.; Villa, A. Magnesium Ion-Water Coordination and Exchange in Biomolecular Simulations. *J. Chem. Theory Comput.* **2012**, *8*, 1493−1502.
(45) Cieplak, P.; Cornell, W. D.; Bayly, C.; Kollman, P. A. Application of the Multimolecule and Multiconformational Resp Methodology to Biopolymers - Charge Derivation for DNA, Rna, and Proteins. *J. Comput. Chem.* **1995**, *16*, 1357−1377.
(46) Cornell, W. D.; Cieplak, P.; Bayly, C. I.; Kollmann, P. A. Application of Resp Charges to Calculate Conformational Energies, Hydrogen-Bond Energies, and Free-Energies of Solvation. *J. Am. Chem. Soc.* **1993**, *115*, 9620−9631.
(47) Jorgensen, W. L.; Chandrasekhar, J.; Madura, J. D.; Impey, R. W.; Klein, M. L. Comparison of Simple Potential Functions for Simulating Liquid Water. *J. Chem. Phys.* **1983**, *79*, 926−935.
(48) Gordon, J. C.; Myers, J. B.; Folta, T.; Shoja, V.; Heath, L. S.; Onufriev, A. H++: A Server for Estimating pK_as and Adding Missing Hydrogens to Macromolecules. *Nucleic Acids Res.* **2005**, *33*, W368−W371.
(49) Leach, A. R. *Molecular Modelling: Principles and Applications*, Second ed.; Pearson Education Limited: Essex, 2001.
(50) Allen, M. P.; Tildesley, D. J. *Computer Simulations of Liquids*; Clarendon Press: Oxford, UK, 1987.
(51) York, D. M.; Darden, T. A.; Pedersen, L. G. The Effect of Long-Range Electrostatic Interactions in Simulations of Macromolecular Crystals - a Comparison of the Ewald and Truncated List Methods. *J. Chem. Phys.* **1993**, *99*, 8345−8348.
(52) Ryckaert, J. P.; Ciccotti, G.; Berendsen, H. J. C. Numerical Integration of the Cartesian Equations of Motion of a System with Constraints: Molecular Dynamics of n-Alkanes. *J. Comput. Phys.* **1977**, *23*, 327−341.
(53) Weiser, J.; Shenkin, P. S.; Still, W. C. Approximate Atomic Surfaces from Linear Combinations of Pairwise Overlaps (LCPO). *J. Comput. Chem.* **1999**, *20*, 217−230.
(54) Suarez, S. C.; Beardslee, R. A.; Toffton, S. M.; McCulloch, S. D. Biochemical Analysis of Active Site Mutations of Human Polymerase *η*. *Mutat. Res., Fundam. Mol. Mech. Mutagen.* **2013**, *745*, 46−54.
(55) Glick, E.; Chau, J. S.; Vigna, K. L.; McCulloch, S. D.; Adman, E. T.; Kunkel, T. A.; Loeb, L. A. Amino Acid Substitutions at Conserved Tyrosine 52 Alter Fidelity and Bypass Efficiency of Human DNA Polymerase *η*. *J. Biol. Chem.* **2003**, *278*, 19341−19346.
(56) Crowley, P. B.; Golovin, A. Cation-Pi Interactions in Protein-Protein Interfaces. *Proteins: Struct., Funct., Genet.* **2005**, *59*, 231−239.
(57) Gallivan, J. P.; Dougherty, D. A. Cation-Pi Interactions in Structural Biology. *Proc. Natl. Acad. Sci. U. S. A.* **1999**, *96*, 9459−9464.
(58) Alt, A.; Lammens, K.; Chiocchini, C.; Lammens, A.; Pieck, J. C.; Kuch, D.; Hopfner, K. P.; Carell, T. Bypass of DNA Lesions Generated During Anticancer Treatment with Cisplatin by DNA Polymerase *η*. *Science* **2007**, *318*, 967−970.
(59) Ucisik, M. N.; Hammes-Schiffer, S. Relative Binding Free Energies of Adenine and Guanine to Damaged and Undamaged DNA in Human DNA Polymerase *η*: Clues for Fidelity and Overall Efficiency. *J. Am. Chem. Soc.* **2015**, *137*, 13240−13243.

DOI: 10.1021/acs.jcim.5b00606
J. Chem. Inf. Model. 2015, 55, 2672−2681